Electronic Supplementary Material (ESI) for Physical Chemistry Chemical Physics.
This journal is © the Owner Societies 2023

Soft Phonon Modes Lead to Suppressed Thermal Conductivity in Ag-Based Chalcopyrites under High Pressure

Kunpeng Yuan[1], Xiaoliang Zhang[2*], Yufei Gao[2], Dawei Tang[2*]

[1]*College of New Energy, China University of Petroleum (East China), Qingdao 266580, China.*

[2]*Key Laboratory of Ocean Energy Utilization and Energy Conservation of Ministry of Education, School of Energy and Power Engineering, Dalian University of Technology, Dalian 116024, China.*

[*]*Corresponding author. zhangxiaoliang@dlut.edu.cn (X.Z.); dwtang@dlut.edu.cn (D.T.)*

Table S1. Calculated lattice constants compared with experimental values.[1]

	Pressure	This work		Experiment	
		a (Å)	*c* (Å)	*a* (Å)	*c* (Å)
$AgAlS_2$	0 GPa	5.63	10.44	5.69	10.24
	3 GPa	5.57	10.28		
$AgAlSe_2$	0 GPa	5.91	11.03	5.95	10.71
	3 GPa	5.84	10.82		
$AgAlTe_2$	0 GPa	6.28	12.12	6.29	11.83
	3 GPa	6.18	11.88		
$AgGaS_2$	0 GPa	5.65	10.49	5.74	10.27
	3 GPa	5.59	10.30		
$AgGaSe_2$	0 GPa	5.91	11.10	5.97	10.87
	3 GPa	5.85	10.87		
$AgGaTe_2$	0 GPa	6.27	12.13	6.29	11.95
	3 GPa	6.16	11.88		
$AgInS_2$	0 GPa	5.80	11.33	5.81	11.16
	3 GPa	5.72	11.16		
$AgInSe_2$	0 GPa	6.06	11.89	6.09	11.69
	3 GPa	5.97	11.67		
$AgInTe_2$	0 GPa	6.43	12.77	6.44	12.634
	3 GPa	6.31	12.52		

Table S2. Calculated bond lengths of Ag-Y and X-Y, and type I and II bond angles of Y-Ag-Y, Y-X-Y, and Ag-Y-X.

	Pressure	Bond length		Bond angle					
		Ag-Y (Å)	X-Y (Å)	Y-Ag-Y (I)	Y-Ag-Y (II)	Y-X-Y (I)	Y-X-Y (II)	Ag-Y-X (I)	Ag-Y-X (II)
$AgAlS_2$	0 GPa	2.51	2.26	117.29°	105.71°	109.49°	109.46°	112.91°	107.01°
	3 GPa	**2.47**	**2.24**	**117.40°**	**105.66°**	**109.94°**	**109.24°**	**113.22°**	**106.92°**
$AgAlSe_2$	0 GPa	2.61	2.40	116.20°	106.21°	109.95°	109.23°	112.77°	107.36°
	3 GPa	**2.57**	**2.37**	**116.48°**	**106.08°**	**110.50°**	**108.96°**	**113.21°**	**107.18°**
$AgAlTe_2$	0 GPa	2.75	2.63	113.03°	107.72°	109.79°	109.31°	111.33°	108.42°
	3 GPa	**2.69**	**2.59**	**113.12°**	**107.68°**	**110.08°**	**109.17°**	**111.53°**	**108.34°**
$AgGaS_2$	0 GPa	2.50	2.29	116.70°	105.98°	110.07°	109.17°	113.04°	107.17°
	3 GPa	**2.46**	**2.26**	**116.97°**	**105.86°**	**110.62°**	**108.90°**	**113.47°**	**107.00°**
$AgGaSe_2$	0 GPa	2.60	2.43	115.43°	106.57°	110.21°	109.11°	112.61°	107.59°
	3 GPa	**2.56**	**2.39**	**115.85°**	**106.38°**	**110.83°**	**108.80°**	**113.14°**	**107.35°**
$AgGaTe_2$	0 GPa	2.73	2.64	112.60°	107.93°	109.79°	109.31°	111.14°	108.55°
	3 GPa	**2.68**	**2.59**	**112.80°**	**107.83°**	**110.09°**	**109.16°**	**111.39°**	**108.43°**
$AgInS_2$	0 GPa	2.51	2.48	111.18°	108.62°	110.24°	109.09°	110.70°	108.85°
	3 GPa	**2.46**	**2.45**	**111.06°**	**108.68°**	**110.54°**	**108.94°**	**110.80°**	**108.81°**
$AgInSe_2$	0 GPa	2.60	2.61	110.49°	108.96°	110.58°	108.92°	110.54°	108.94°
	3 GPa	**2.56**	**2.57**	**110.46°**	**108.98°**	**110.90°**	**108.76°**	**110.68°**	**108.87°**
$AgInTe_2$	0 GPa	2.74	2.81	108.89°	109.76	110.82	108.80	109.83°	109.25°
	3 GPa	**2.69**	**2.76**	**108.80°**	**109.81**	**110.98**	**108.72**	**109.86°**	**109.22°**

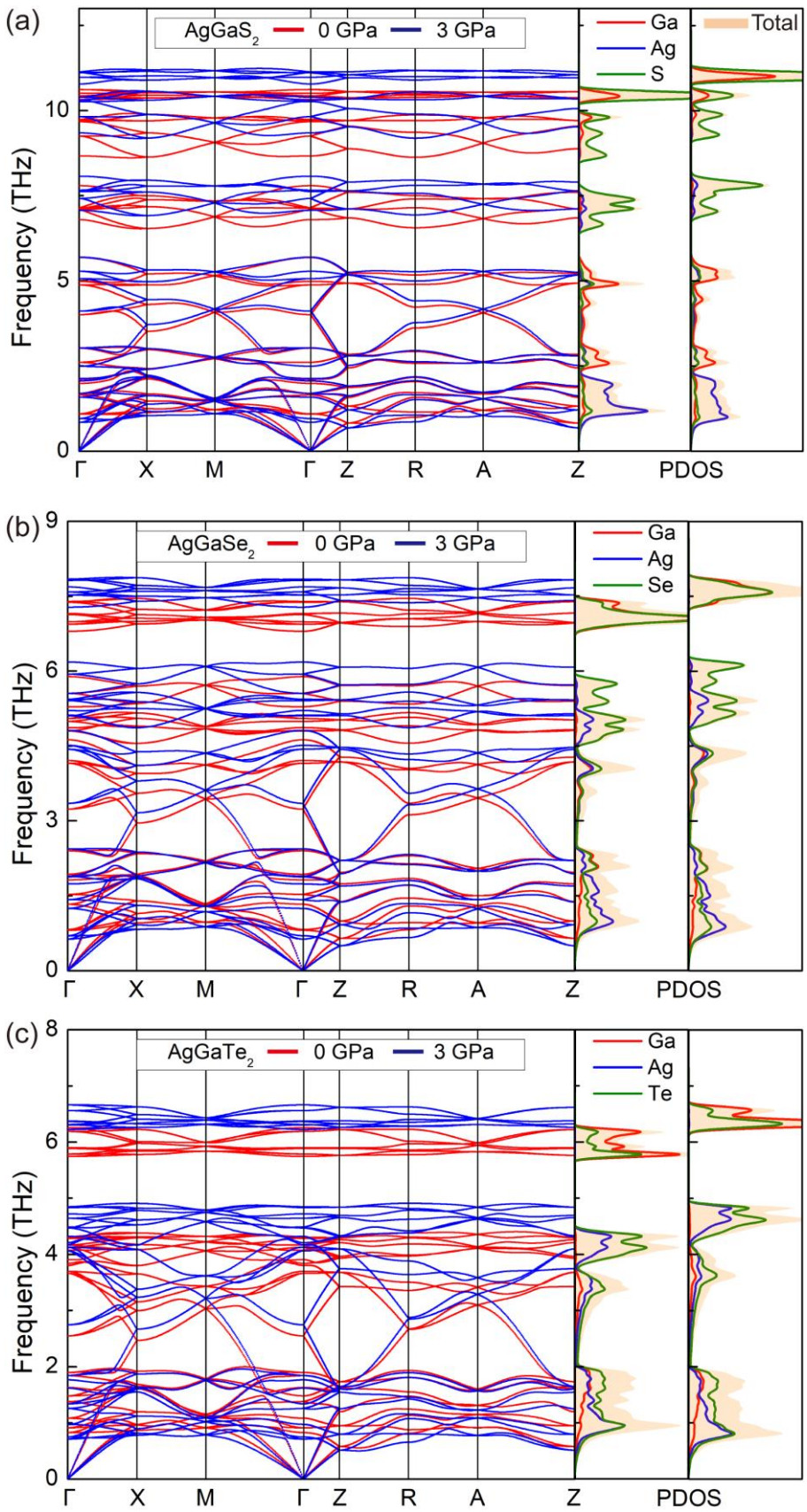

Figure S1. Phonon dispersions and atom-decomposed density of states (PDOS) of (a) $AgGaS_2$, (b) $AgGaSe_2$, and (c) $AgGaTe_2$.

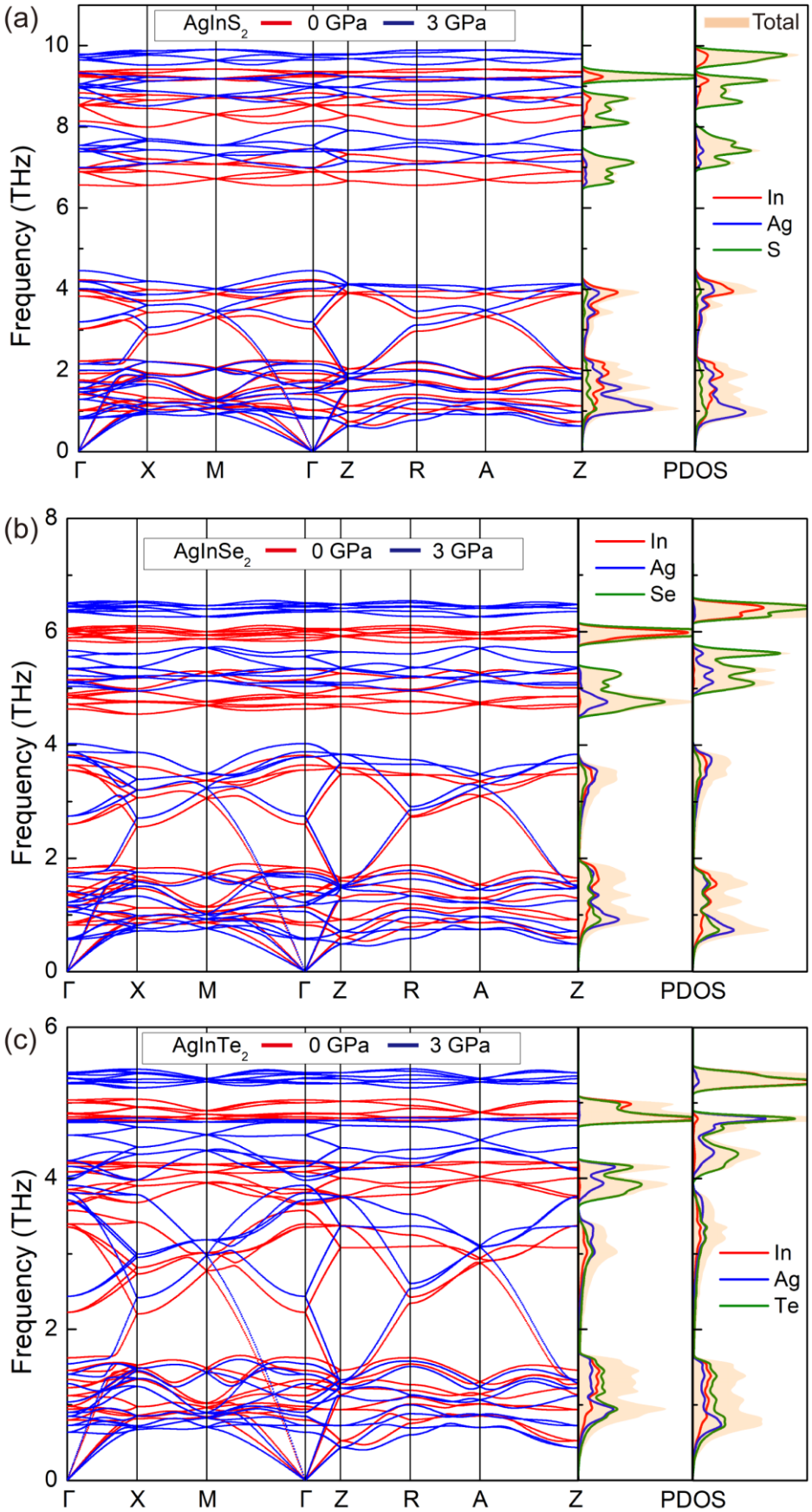

Figure S2. Phonon dispersions and atom-decomposed density of states (PDOS) of (a) $AgInS_2$, (b) $AgInSe_2$, and (c) $AgInTe_2$.

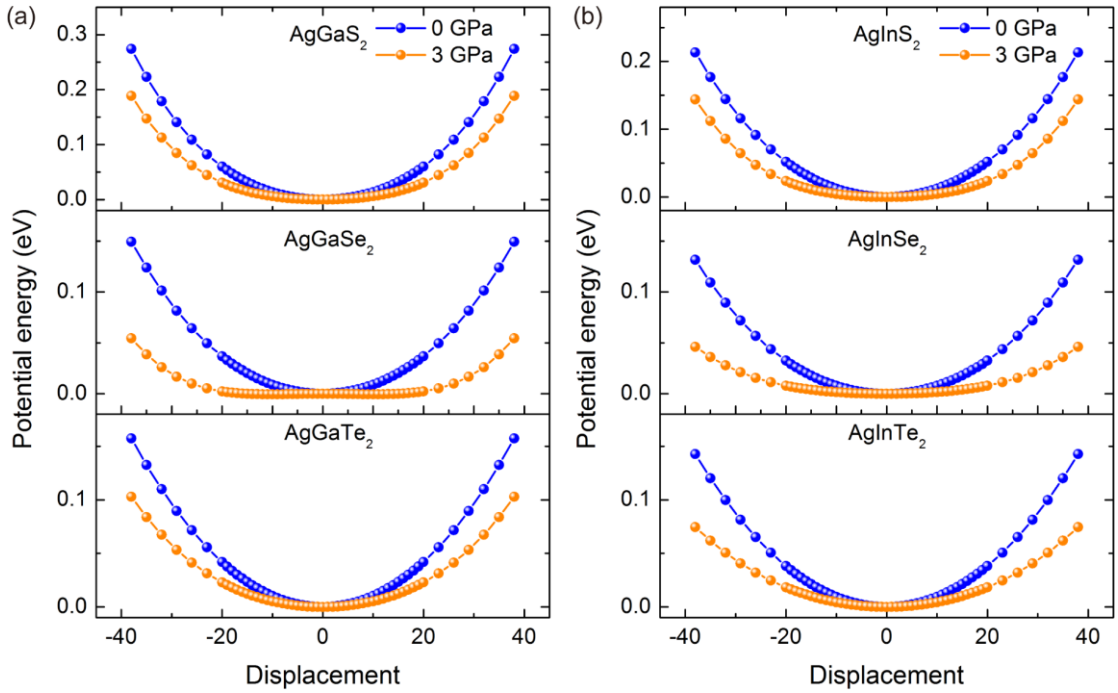

Figure S3. Potential energy variation as a function of displacement for lowest transverse optical mode at the *Γ* point for (a) $AgGaS_2$, $AgGaSe_2$, and $AgGaTe_2$, and (b) for $AgInS_2$, $AgInSe_2$, and $AgInTe_2$.

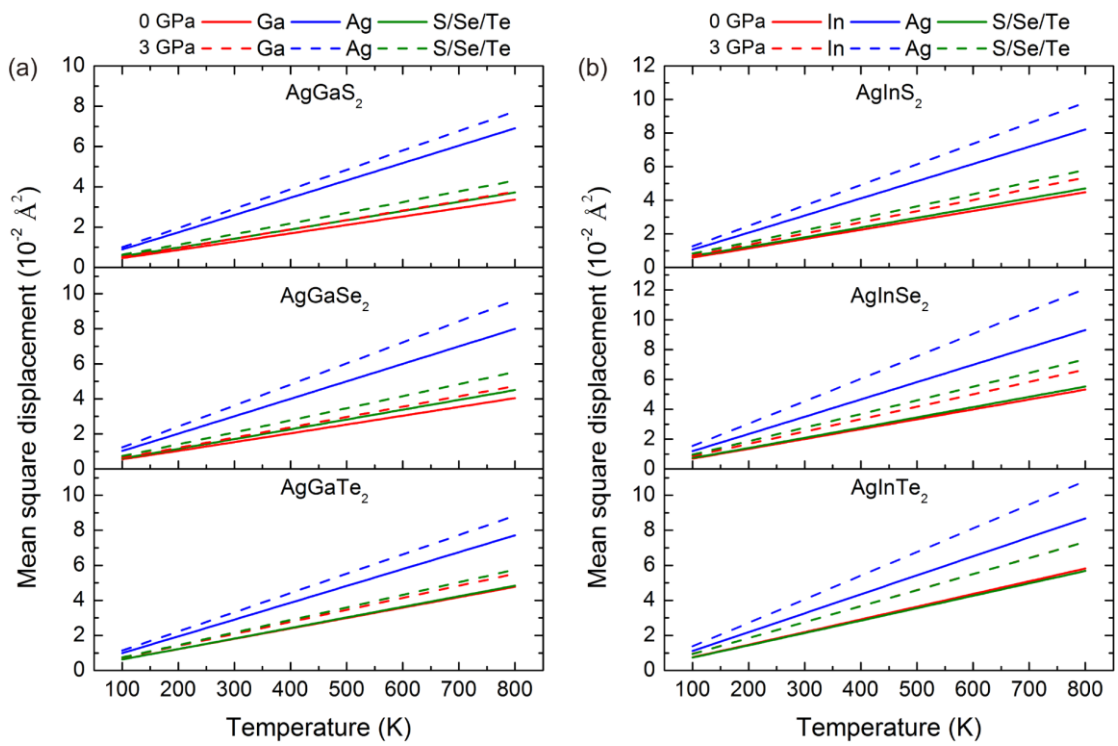

Figure S4. Temperature-dependent mean square displacement for (a) $AgGaS_2$, $AgGaSe_2$, and $AgGaTe_2$, and (b) for $AgInS_2$, $AgInSe_2$, and $AgInTe_2$.

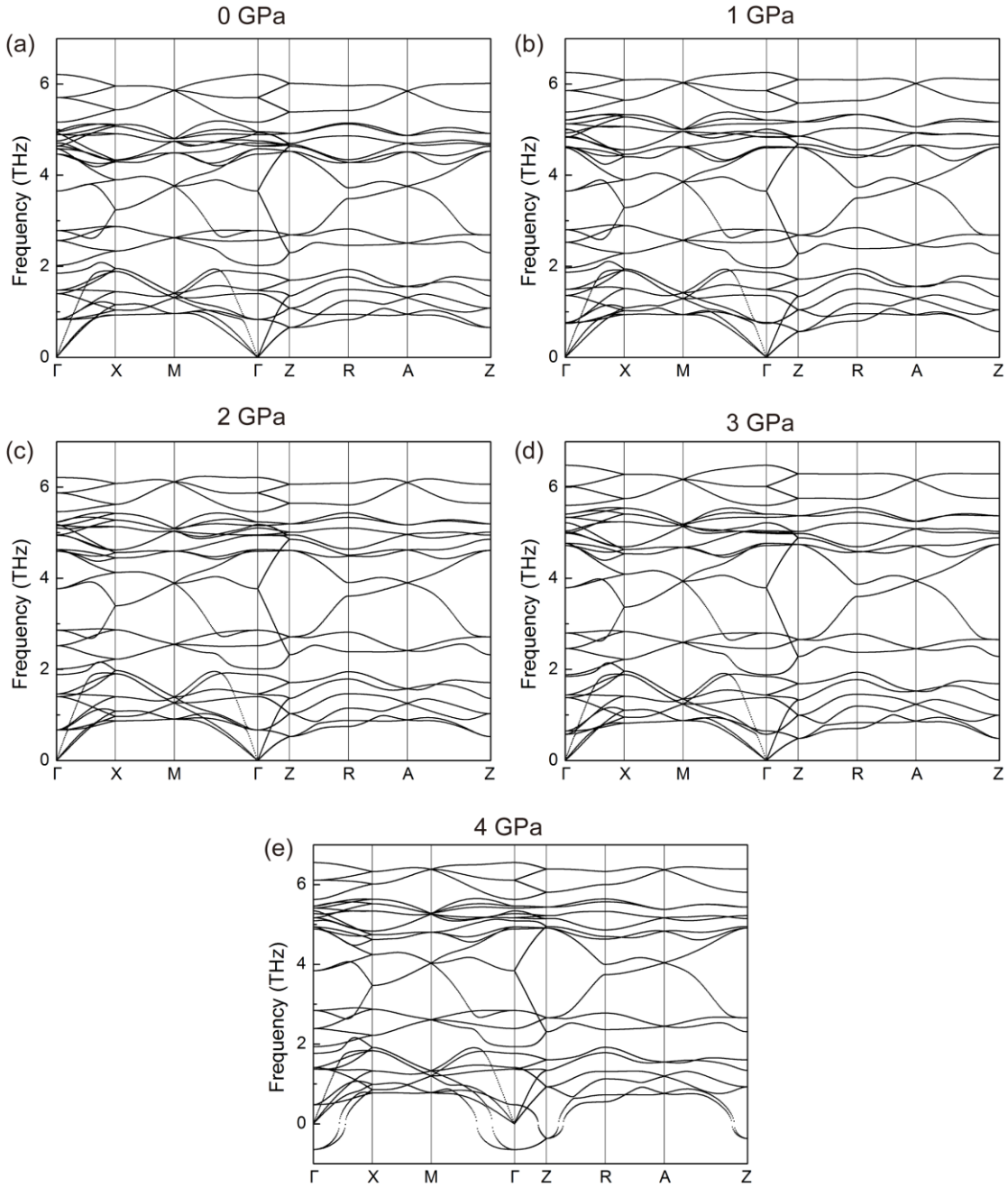

Figure S5. Pressure-dependent phonon dispersions of $AgAlSe_2$. (a) 0 GPa, (b) 1 GPa, (c) 2 GPa, (d) 3 GPa, and (e) 4 GPa.

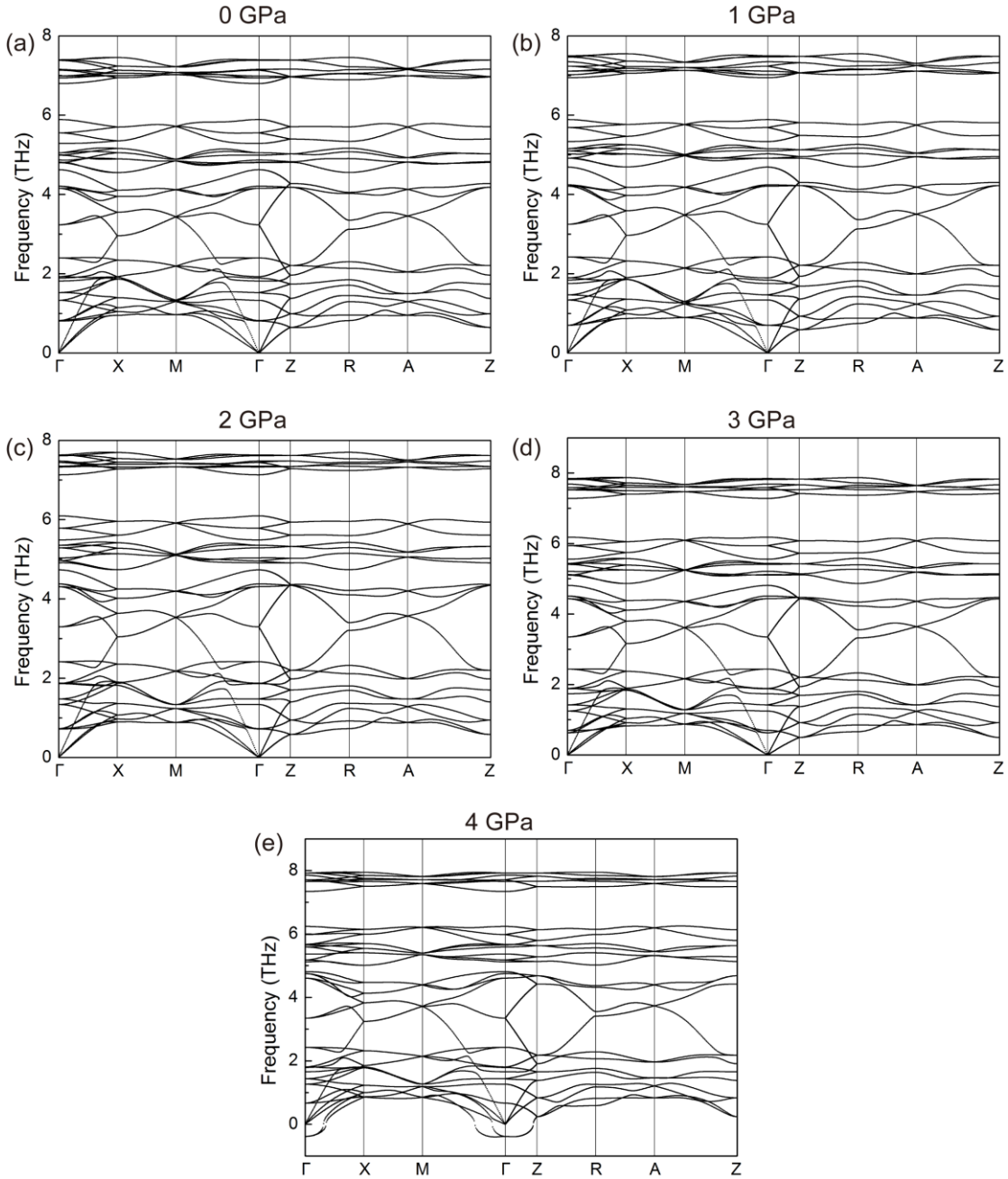

Figure S6. Pressure-dependent phonon dispersions of $AgGaSe_2$. (a) 0 GPa, (b) 1 GPa, (c) 2 GPa, (d) 3 GPa, and (e) 4 GPa.

Table S3. The calculated thermal conductivity compared with experimental and simulation results. The calculated thermal conductivity is averaged over three directions.

	Thermal conductivity (W/mK)		
	This work	Experiment	Simulation[2]
$AgAlS_2$	1.71	-	2.03
$AgAlSe_2$	1.33	-	0.94
$AgAlTe_2$	2.25	-	1.46
$AgGaS_2$	2.24	1.4[3]	2.23
$AgGaSe_2$	1.33	1.2[4]	0.77
$AgGaTe_2$	2.60	1.94[5]	1.43
$AgInS_2$	2.35	-	2.05
$AgInSe_2$	1.92	1.1[6]	0.89
$AgInTe_2$	2.48	2.05[5]	1.69

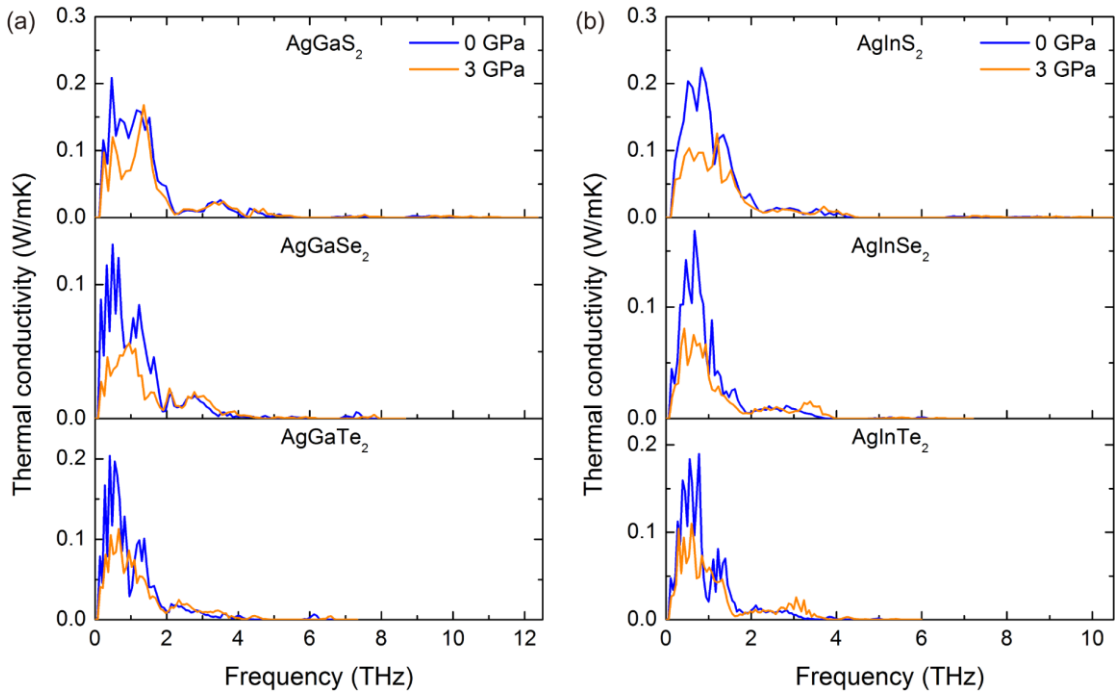

Figure S7. Frequency decomposed thermal conductivity for (a) $AgGaS_2$, $AgGaSe_2$, and $AgGaTe_2$, and (b) for $AgInS_2$, $AgInSe_2$, and $AgInTe_2$ at 0 GPa and 3 GPa.

Table S4. The percentage contribution of phonons in different frequency ranges to thermal conductivity.

	Percentage contribution (%)			
	0-2 THz		0-1 THz	
	0 GPa	3 GPa	0 GPa	3 GPa
$AgAlS_2$	77.86	72.73	41.87	34.35
$AgAlSe_2$	81.02	70.64	54.31	50.65
$AgAlTe_2$	83.73	81.55	59.86	58.81
$AgGaS_2$	85.33	79.83	47.97	40.70
$AgGaSe_2$	85.46	74.54	53.08	46.94
$AgGaTe_2$	88.98	81.65	61.14	58.76
$AgInS_2$	90.30	84.91	62.95	53.05
$AgInSe_2$	90.41	81.52	70.23	64.65
$AgInTe_2$	91.38	82.65	67.91	63.54

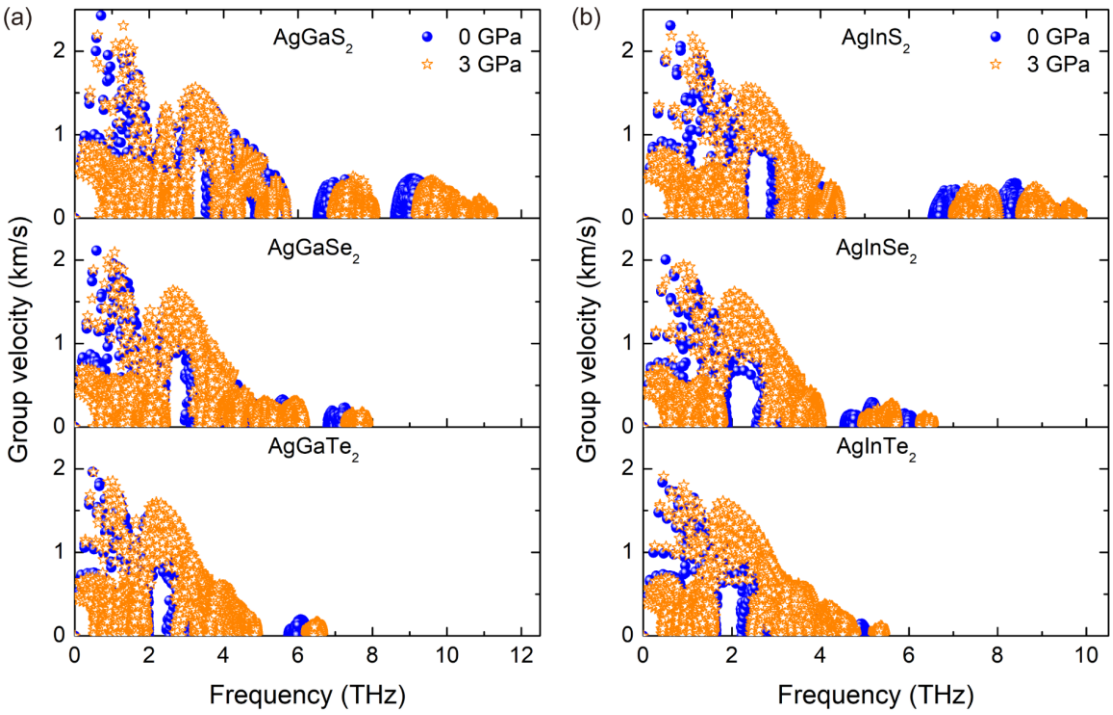

Figure S8. Phonon group velocity for (a) $AgGaS_2$, $AgGaSe_2$, and $AgGaTe_2$, and (b) for $AgInS_2$, $AgInSe_2$, and $AgInTe_2$ at 0 GPa and 3 GPa.

Table S5. Calculated group velocities of transverse acoustic (TA) and longitudinal acoustic (LA) phonons around the *Γ* point for two representative pressures.

	Pressure	*Γ-X*			*Γ-Z*		
		v_{TA1} (m/s)	v_{TA2} (m/s)	v_{LA} (m/s)	v_{TA1} (m/s)	v_{TA1} (m/s)	v_{LA} (m/s)
$AgAlS_2$	0 GPa	2062	2581	4830	2062	2062	4625
	3 GPa	1510	2312	5117	1510	1510	4793
	$(v_{3GPa}-v_{0GPa})/v_{0GPa}$ (%)	-26.75	-10.43	5.94	-26.75	-26.75	3.64
$AgAlSe_2$	0 GPa	1775	1962	3990	1775	1775	3767
	3 GPa	1360	1825	4082	1360	1360	3841
	$(v_{3GPa}-v_{0GPa})/v_{0GPa}$ (%)	-23.42	-6.98	2.31	-23.42	-23.42	1.98
$AgAlTe_2$	0 GPa	1629	1665	3456	1629	1629	3357
	3 GPa	1482	1562	3702	1482	1482	3570
	$(v_{3GPa}-v_{0GPa})/v_{0GPa}$ (%)	-9.07	-6.17	7.11	-9.07	-9.07	6.33
$AgGaS_2$	0 GPa	1996	2257	4371	1996	1996	4175
	3 GPa	1591	2119	4614	1591	1591	4375
	$(v_{3GPa}-v_{0GPa})/v_{0GPa}$ (%)	-20.29	-6.12	5.55	-20.29	-20.29	4.79
$AgGaSe_2$	0 GPa	1684	1901	3738	1684	1684	3573
	3 GPa	1222	1653	4009	1222	1222	3702
	$(v_{3GPa}-v_{0GPa})/v_{0GPa}$ (%)	-27.45	-13.07	7.25	-27.45	-27.45	3.61
$AgGaTe_2$	0 GPa	1492	1591	3304	1492	1492	3187
	3 GPa	1289	1478	3470	1289	1289	3372
	$(v_{3GPa}-v_{0GPa})/v_{0GPa}$ (%)	-13.61	-7.70	5.03	-13.61	-13.61	5.80
$AgInS_2$	0 GPa	1819	1830	3878	1819	1819	3788
	3 GPa	1563	1657	4086	1563	1563	3974
	$(v_{3GPa}-v_{0GPa})/v_{0GPa}$ (%)	-14.09	-9.43	5.38	-14.09	-14.09	4.91
$AgInSe_2$	0 GPa	1523	1535	3318	1535	1535	3294
	3 GPa	1329	1373	3461	1373	1373	3420
	$(v_{3GPa}-v_{0GPa})/v_{0GPa}$ (%)	-12.74	-10.51	4.30	-10.51	-10.51	3.83
$AgInTe_2$	0 GPa	1418	1424	2992	1418	1418	3001

3 GPa	1146	1295	3209	1146	1146	3244
$(\upsilon_{3GPa}-\upsilon_{0GPa})/\upsilon_{0GPa}$ (%)	-19.17	-9.09	7.25	-19.17	-19.17	8.10

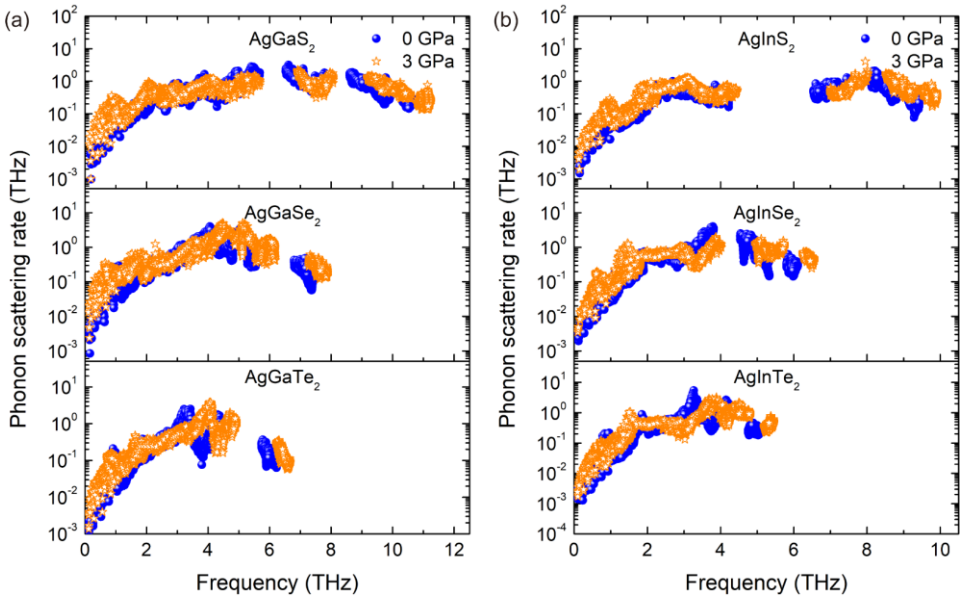

Figure S9 Phonon scattering rate for (a) $AgGaS_2$, $AgGaSe_2$, and $AgGaTe_2$, and (b) for $AgInS_2$, $AgInSe_2$, and $AgInTe_2$ at 0 GPa and 3 GPa.

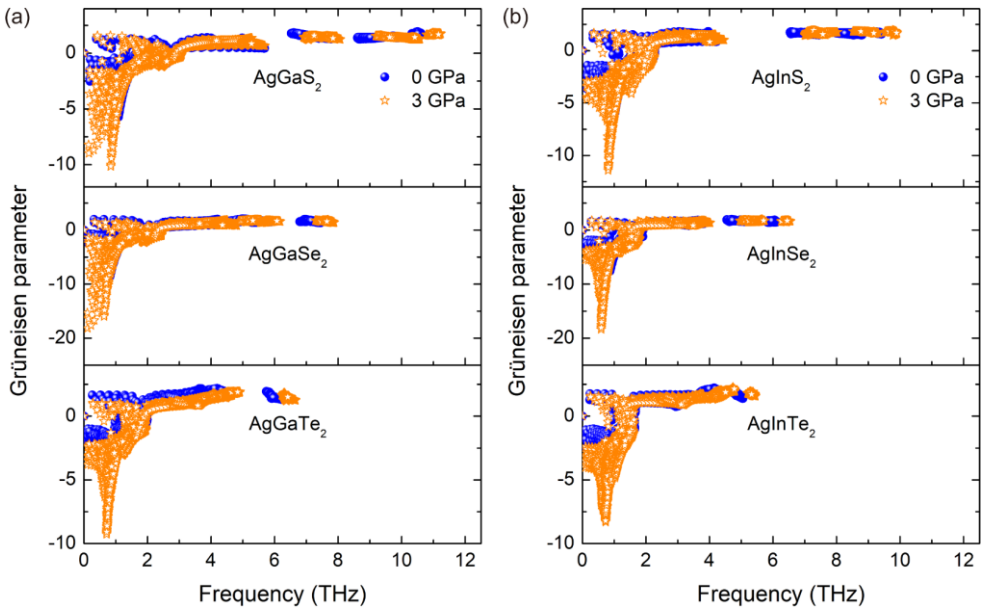

Figure S10. Grüneisen parameter for (a) $AgGaS_2$, $AgGaSe_2$, and $AgGaTe_2$, and (b) for $AgInS_2$, $AgInSe_2$, and $AgInTe_2$ at 0 GPa and 3 GPa.

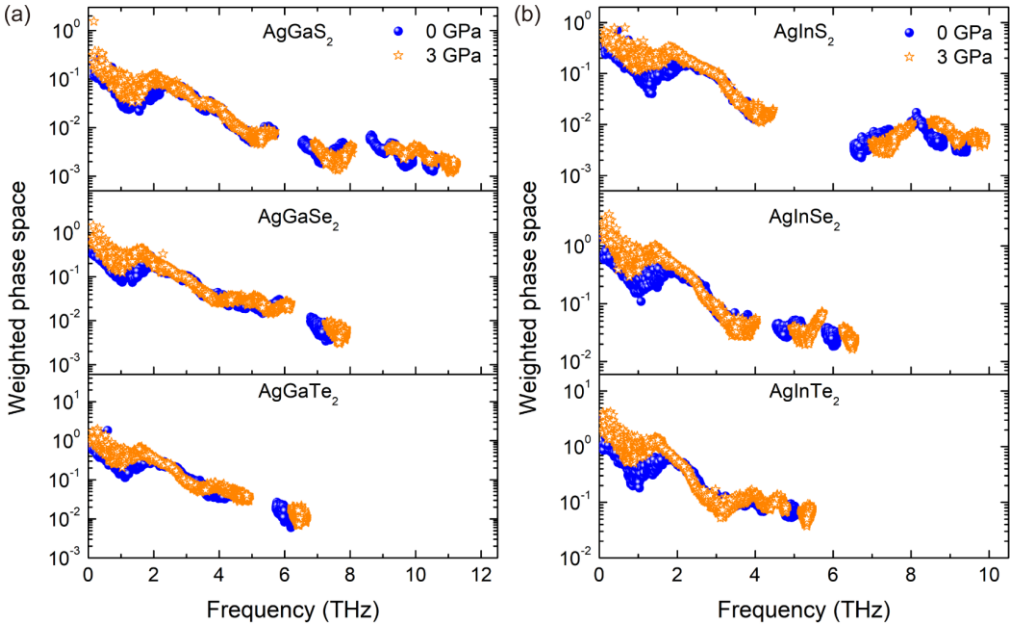

Figure S11. Weighted scattering phase space for (a) $AgGaS_2$, $AgGaSe_2$, and $AgGaTe_2$, and (b) for $AgInS_2$, $AgInSe_2$, and $AgInTe_2$ at 0 GPa and 3 GPa.

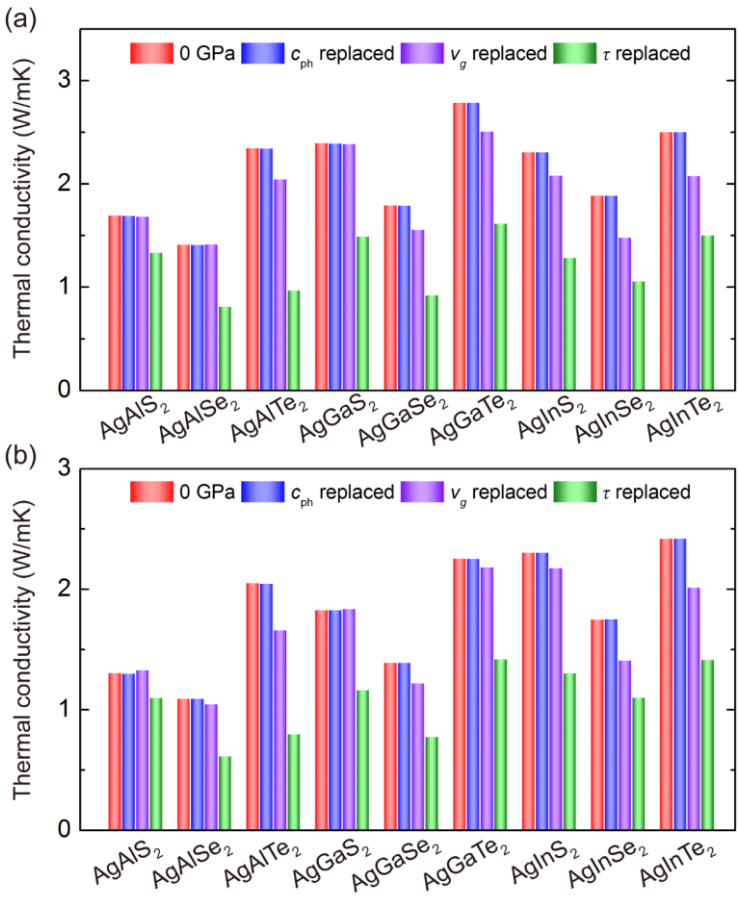

Figure S12. Cross-calculated thermal conductivity along the (a) *a*/*b* and (b) *c* axis with phonon specific heat c_{ph}, group velocity v_g, and relaxation time τ replaced with high-pressure values.

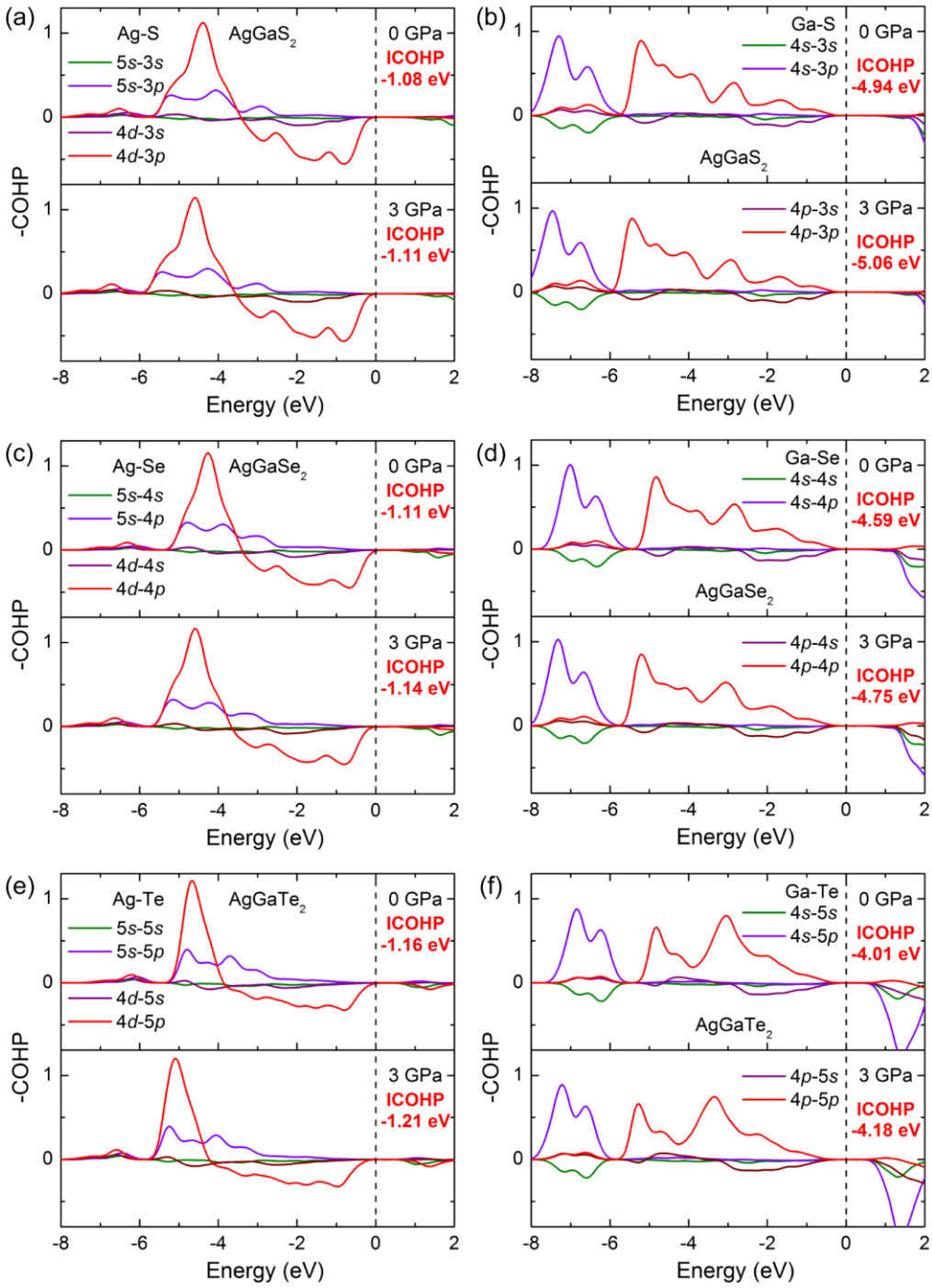

Figure S13. The calculated COHP for the Ag-Y and Ga-Y bonds of $AgGaS_2$, $AgGaSe_2$, and $AgGaTe_2$ at 0 GPa and 3 GPa. (a) Ag-S, (b) Ga-S, (c) Ag-Se, (d) Ga-Se, (e) Ag-Te, and (f) Ga-Te.

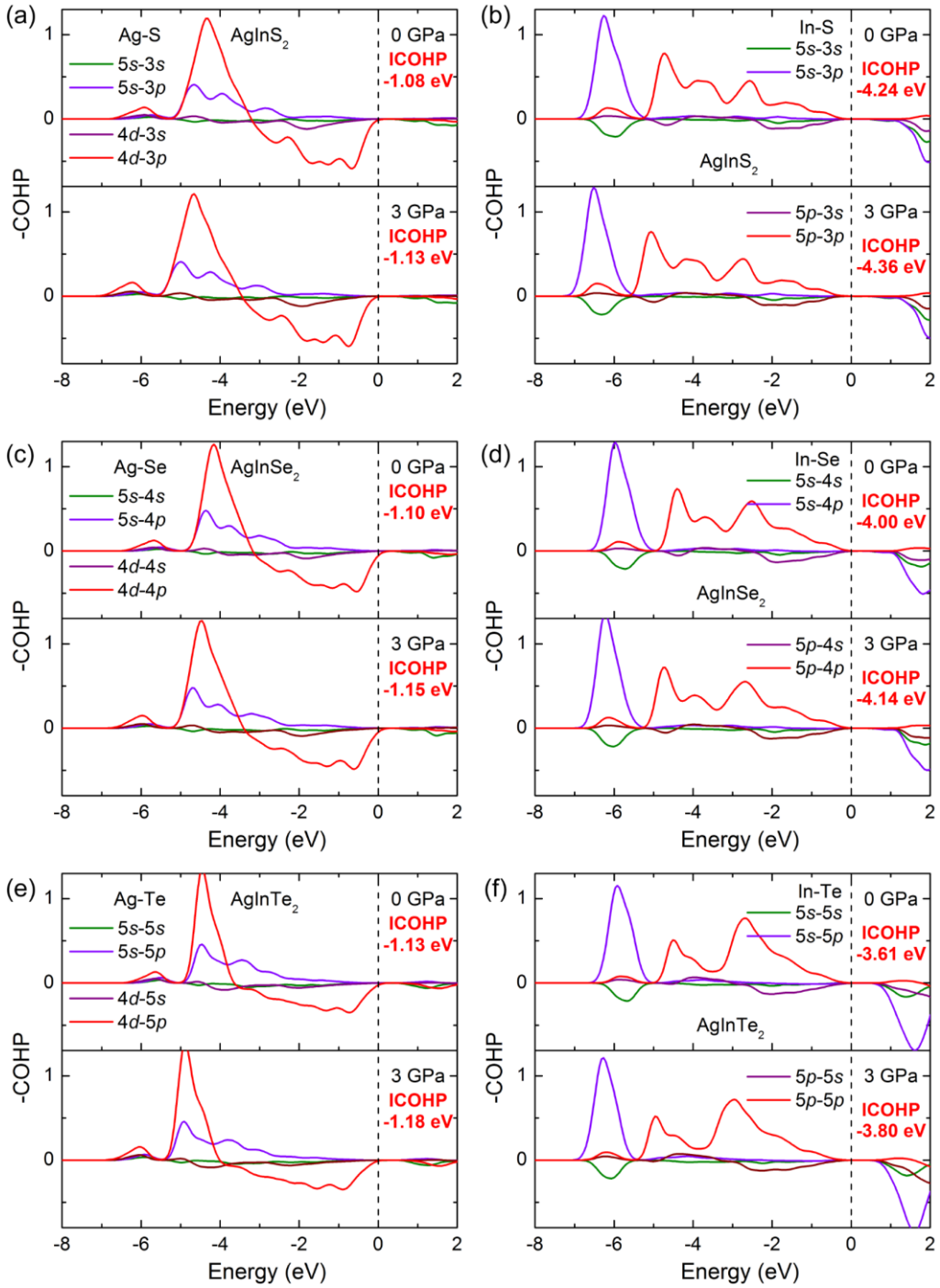

Figure S14. The calculated COHP for the Ag-Y and In-Y bonds of $AgInS_2$, $AgInSe_2$, and $AgInTe_2$ at 0 GPa and 3 GPa. (a) Ag-S, (b) In-S, (c) Ag-Se, (d) In-Se, (e) Ag-Te, and (f) In-Te.

Table S6. The transferred and shared electrons between atoms in $AgXY_2$ (X = Al, Ga, In; Y = S, Se, Te).

	Pressure	Transferred electron |e|			Shared electron |e|	
		Ag	X^{III}	Y^{VI}	Ag-Y^{VI}	X^{III}-Y^{VI}
$AgAlS_2$	0 GPa	0.424	1.102	-0.763	0.884	1.002
	3 GPa	0.438	1.114	-0.776	0.926	1.016
$AgAlSe_2$	0 GPa	0.352	0.904	-0.628	0.891	1.023
	3 GPa	0.365	0.923	-0.644	0.939	1.041
$AgAlTe_2$	0 GPa	0.225	0.606	-0.415	0.971	1.055
	3 GPa	0.238	0.633	-0.435	1.031	0.082
$AgGaS_2$	0 GPa	0.367	0.806	-0.587	0.904	1.070
	3 GPa	0.378	0.811	-0.594	0.944	1.097
$AgGaSe_2$	0 GPa	0.290	0.638	-0.464	0.917	1.051
	3 GPa	0.297	0.643	-0.470	0.962	1.085
$AgGaTe_2$	0 GPa	0.153	0.403	-0.278	1.000	1.047
	3 GPa	0.159	0.408	-0.284	1.059	1.092
$AgInS_2$	0 GPa	0.370	0.893	-0.631	0.924	1.043
	3 GPa	0.380	0.898	-0.639	0.975	1.075
$AgInSe_2$	0 GPa	0.302	0.737	-0.519	0.933	1.028
	3 GPa	0.308	0.742	-0.525	0.989	1.068
$AgInTe_2$	0 GPa	0.178	0.520	-0.349	1.002	1.032
	3 GPa	0.184	0.524	-0.354	1.071	1.084

References

1. Shay, J. L.; Wernick, J. H., Ternary chalcopyrite semiconductors: growth, electronic properties, and applications. Pergamon: Oxford, U.K., 1975.

2. Plata, J. J.; Posligua, V.; Márquez, A. M.; Fernandez Sanz, J.; Grau-Crespo, R., Charting the lattice thermal conductivities of I–III–VI_2 chalcopyrite semiconductors. *Chemistry of Materials* 2022, 34, 2833-2841.

3. Catella, G. C.; Burlage, D., Crystal growth and optical properties of $AgGaS_2$ and $AgGaSe_2$. *MRS Bulletin* 2013, 23, 28-36.

4. Aggarwal, R. L.; Fan, T. Y., Thermal diffusivity, specific heat, thermal conductivity, coefficient of thermal expansion, and refractive-index change with temperature in $AgGaSe_2$. *Applied Optics* 2005, 44, 2673-2677.

5. Charoenphakdee, A.; Kurosaki, K.; Muta, H.; Uno, M.; Yamanaka, S., Thermal conductivity of the ternary compounds: $AgMTe_2$ and AgM_5Te_8 (M = Ga or In). *Materials Transactions* 2009, 50, 1603-1606.

6. Qiu, P.; Qin, Y.; Zhang, Q.; Li, R.; Yang, J.; Song, Q.; Tang, Y.; Bai, S.; Shi, X.; Chen, L., Intrinsically high thermoelectric performance in $AgInSe_2$ n-type diamond-like compounds. *Advanced Science* 2018, 5, 1700727.